J. Eur. Opt. Society-Rapid Publ. 2023, **19**, 26

https://doi.org/10.1051/jeos/2023022
Available online at: https://jeos.edpsciences.org

Journal of the European Optical Society-Rapid Publications

Special Issue - EOSAM 2022
Guest editors: Patricia Segonds, Gilles Pauliat and Emiliano Descrovi

RESEARCH ARTICLE OPEN ACCESS

Linearly modulated multi-focal diffractive lens for multi-sheet excitation of flow driven samples in a light-sheet fluorescence microscope

Meike Hofmann[1,*], Shima Gharbi Ghebjagh[1], Yuchao Feng[1], Chao Fan[1], Karen Lemke[2], and Stefan Sinzinger[1]

[1] Technische Universität Ilmenau, Fachgebiet Technische Optik, Postfach 100565, 98684 Ilmenau, Germany
[2] Iba Heiligenstadt, 37308 Heilbad Heiligenstadt, Germany

Received 15 February 2023 / Accepted 19 April 2023

Abstract. Light sheet fluorescence microscope with single light sheet illumination enables rapid 3D imaging of living cells. In this paper we show the design, fabrication and characterization of a diffractive optical element producing several light sheets along a 45° inclined tube. The element, which is based on a multi-focal diffractive lens and a linear grating, generates five thin light sheets with equal intensities when combined with a refractive cylindrical lens. The generated uniform light sheets can be applied for the scanning of samples in tubes enabling flow-driven 3-dimensional imaging.

Keywords: Light sheet fluorescence microscopy, Diffractive optical elements, Multi-plane imaging, 3D imaging, Multi-focal lens.

1 Introduction

Light sheet fluorescence microscopy (LSFM) is a kind of Selective plane illumination microscopy (SPIM). Commonly, the single light-sheet fluorescence microscope is used, which divides the fluorescence excitation and detection optical paths into two perpendicular parts. Only the sample located in the focal plane of the detection objective is illuminated by the thin laser light sheet produced by the optical system [1]. LSFM improves the imaging speed significantly in comparison to confocal microscopes, by applying side-illuminated surface imaging method [2]. Illuminating the sample only in a specific area reduces the sample phototoxicity and allows the sample to be imaged over a long period of time [1, 3].

In conventional LSFM the light sheet that is produced directly by lasers and cylindrical lenses has the Gaussian distribution characteristics [4]. In order to improve the axial resolution and the imaging speed, the size of the light sheet should be reduced as much as possible. But a light sheet that is too short leads to a narrower field of view, especially in single light sheet fluorescence microscopy. In order to solve this contradiction other structured light forms have been applied to the system such as Bessel beams. Ideally this nondiffracting beams would produce a thinner and more uniform beam. However, in practice, only Bessel–Gaussian beams can be obtained due to the inability to obtain infinitely narrow annular beams. The narrower light sheets have higher energy in the side lobes [5], with increased phototoxicity.

In recent years, there have been many optimizations in the structure of light-sheet microscopes, as well as in sample fixation and culture methods. One important step is the development from 2D to the 3D cell cultivation. Due to their tissue-specific in vivo situation, 3D cell cultures like spheroids or organoids are more realistically than 2D cell cultures, since the micro-environment of the cells in the tissue composite is taken into account. For example the cells can be placed in an extensible 3D culture platform, which can truly reflect the process of a large number of cell growth and proliferation [6]. This enables real-time 3D imaging of life processes in large numbers of living cells in vitro using multi-light-sheet fluorescence microscopy with low phototoxicity using z-stacks [7, 8]. Multi-plane imaging enables the simultaneous illumination of different sample planes [9] and can effectively reduce the aberration caused by the mechanical motion of the system [10, 11], and reduce the difficulty of matching the light sheet and the objective lens.

Therefore, in LSFM based on multi-focal diffractive lens (MFL), illumination can be applied for long-term fast 3D imaging of a large number of living cells. Combining a

* Corresponding author: meike.hofmann@tu-ilmenau.de

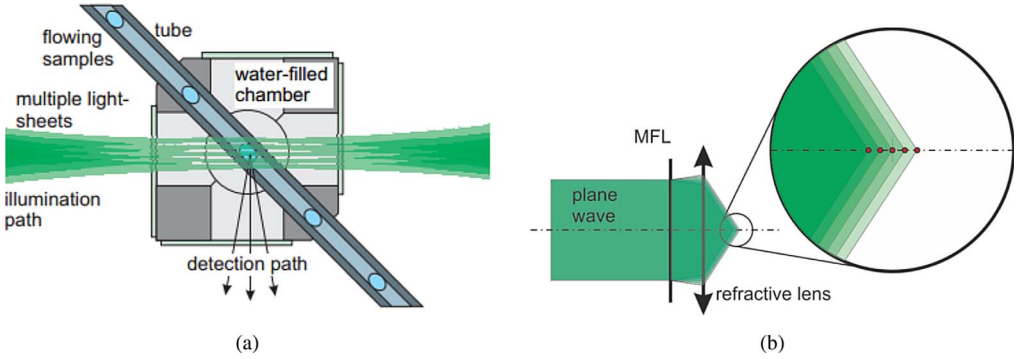

Fig. 1. (a) Schematic of the measurement configuration with tube-guided samples illuminated with multiple light sheets. The inclination of the tube of 45° offers the option of a 90° – detection between illumination and detection path. (b) Resorting of the focal spots by a refractive lens.

MFL with a simple linear grating (LG) results in modulated structured light illumination. For this purpose, the Dammann lens can also produce multiple spots of equal intensity by modulating the transition points. Dammann elements are a special kind of phase elements in which each period is subdivided into different segments with optimized precise widths to generate equal-intensity diffraction orders [12, 13]. However, the fabrication of a Dammann lens is usually very sensitive to changes in transition locations from 0 to π. The most critical issue for the fabrication of Dammann elements is related to the minimum feature size of the technological process. With increasing functionality of the diffractive element performance, the complexity of the element pattern increases and therefore, the requirements on the fabrication process increase respectively. Here, a small change in one of the transition locations causes the intensity distribution between the diffraction orders to vary non-uniformly, as a result of increased zeroth order intensity [14]. As a modification to Dammann method, it is possible to realize the applied nonlinearity as a multi-phase value modulation. Here, the design is accomplished by dividing each period of a pure phase diffractive lens into several areas with equal widths, each having a different phase value. The focus of the design process is based on the optimization of the phase values to acquire the best possible uniformity and efficiency for the generated focal spots as diffraction orders. In comparison to the Dammann lens, MFL has more relaxed fabrication requirements, and therefore is easier to fabricate and produces less errors [15, 16].

Based on the combination of MFL and a simple LG, we have produced a linearly modified multi-focal diffractive lens, shortly named in this paper as DL, for specific area illumination of the 3D culture platform for fluorescence imaging in the laboratory. The dimensions of this platform are 120 mm × 120 mm, in which a guiding tube with flow driven sample passes through at 45°. The platform is filled with water during imaging to match the refractive index of the microscope objective. By placing this DL in an optical system with a 532 nm wavelength laser and a suitable cylindrical lens, five thin light sheets with equal intensities at 1 mm intervals along the guiding tube can be generated to scan the samples. During the imaging process, the 3D culture platform and the guiding tube remain stationary, and the objective lens images the continuous flow driven samples in the guiding tube in the x–y-plane using z-stack imaging (Fig. 1).

2 Design

For the generation of several equal-intensity focal spots along the optical axis with a specific inclined orientation, the combination of a MFL with a LG is used. The combination results is a DL which plays the dual role of a MFL, as a multi-plane defocuser to generate multiple uniform foci, and a beam splitting LG, to re-orient the array of foci along the desired orientation with respect to the optical axis. For this goal, a method based on a detour phase approach is implemented.

The optimized nonlinear phase values in each period of the multi-value element affect the energy distribution in the diffraction orders [16], leading to an efficient equal-intensity array of focus spots. Additionally, a refractive spherical lens behind the DL, rearranges the diffraction orders and defines the locations of the several focal spots and adjusts the distance between them. A refractive cylindrical lens is required, however, to generate uniform multiple light-sheets in the LSFM set-up.

A DL based on MFL and a LG, in combination with a cylindrical lens can generate multiple off-axis light sheets with equal energy distribution along the guiding tube efficiently. In the DL the optimized nonlinear phase values in each period affect the diffraction orders and energy distribution.

The phase function of the MFL can be written as,

$$\phi_{\mathrm{MFL}}(\rho) = \phi[\varphi_d(\rho)] + \varphi_r(\rho), \quad \rho \in [0, R], \tag{1}$$

where ρ is the radius of polar coordinates and R is the element aperture radius.

$$\varphi_d(\rho) = \mathrm{mod}_{2\pi}\left(-\frac{\pi\rho^2}{\lambda f_1}\right), \tag{2}$$

and,

$$\varphi_r(\rho) = -\frac{\pi\rho^2}{\lambda f_2}, \tag{3}$$

describe the phase functions of the diffractive lens and the respective refractive lens with the paraxial focal lengths of f_1 and f_2, respectively. Here λ is the wavelength of illumination. The aim of applying the modulo-function in equation (2) is to restrict the phase to the $[0, 2\pi)$ interval. The function $\phi[\varphi_d(\rho)]$ in equation (1) represents the non-linear transformation of the phase function in diffractive lens, based on a multi phase encoding method. Addition of phase non-linearaties to the structure of a periodic element is a method to achieve additional diffraction orders [17–19]. One simple example of this approach is the binarization of a phase function. In the case of a lens function, binarization generates many local focus points instead of a single focus. In this work we applied a non-linear transformation to the structure of a diffractive lens [20]. The choice of non-linearity function can provide any desired energy distribution among the produced set of foci. The non-linear transformation function here is inspired by the multi-value phase approach. The design is accomplished by dividing each period of an ordinary pure phase element into several areas with equal widths, each having a different phase value. The phase element in our case, is the diffractive lens with annular zones as the discrete periods. The focus of the design process is based on the optimization of the phase values to acquire the best possible uniformity and efficiency for the focal spots [16].

With the expansion of these phase functions into a Fourier series, the illumination beam transmitted through the MFL is regarded as the superposition of spherical beams with focal lengths of,

$$\frac{1}{f_n} = \frac{n}{f_1} + \frac{1}{f_2}, \tag{4}$$

where n represents the corresponding diffraction order.

In the following, we introduce a DL with the following transmission function,

$$T_{\mathrm{DL}}(\rho,\theta) = \sum_{n=-\infty}^{\infty} a_n \exp\left[jn\left(\frac{\pi\rho^2}{\lambda f_1} + \frac{2\pi\rho\cos\theta}{p}\right)\right]\mathrm{circ}\left(\frac{\rho}{\rho_n}\right), \tag{5}$$

where, the Fourier coefficients are defined as,

$$a_n = \begin{cases} \frac{j}{2\pi n}\sum_{m=1}^{N}\exp(j\varphi_m)[\exp(-j2\pi n\rho_m) - \exp(-j2\pi n\rho_{m-1})] & n \neq 0 \\ \sum_{m=1}^{N}\exp(j\varphi_m)[\rho_m - \rho_{m-1}] & n = 0 \end{cases}, \tag{6}$$

the function $\mathrm{circ}(\rho/\rho_n)$ represents a circular mask as,

$$\mathrm{circ}\left(\frac{\rho}{\rho_n}\right) = \begin{cases} 1 & \text{if} \quad \rho \leq \rho_n \\ 0 & \text{if} \quad \rho > \rho_n \end{cases}, \tag{7}$$

where, ρ and θ are the parameters of polar coordinates in input plane, p is the period of the LG and ρ_n are the radii of annular zones of the DL. The parameters N and φ_m are total numbers of unit cells and the optimized phase values, which are assigned to each area of DL to provide multiple foci with uniform intensity level. The LG transmission function rotates the focal spots of MFL around the zeroth order to the desired positions. Therefrom, this DL with cylindrical lens can modulate the parallel illumination laser beam into several thin light sheets along the specimen tube. The optimized phase values in each period of DL determine the desired number and intensity distribution of foci.

For specific area illumination of the 3D culture platform for fluorescence imaging, multiple light sheets (diffraction orders) should be located along the guiding tube in a chamber filled with water, for scanning the flowing samples with specific and equal distances. Regarding the design parameters of the MFL in equation (4), f_2 determines the main refracting power and the location of the focal spot of the zeroth order. The other term, f_1, shifts the higher orders to adjust the distance of the multiple foci.

As mentioned, the design of a MFL is accomplished by dividing the single period of an ordinary diffractive lens into several areas with equal widths, each having a different optimized phase value. For a 1×5 order MFL, it is possible to use some optimization algorithms, such as simulated annealing or genetic algorithm to define the phase values [21–23]. In order to simplify the design and optimization process, it is possible to regard the phase function of a diffraction grating to apply the nonlinearity function and use a semi-analytical design and optimization process. Figure 2 shows the configuration of a single grating unit cell. As a symmetric light distribution is required, the grating unit cell should also have a symmetric profile, thus φ_2 and φ_4 are the same and can be set to zero for simplicity. Another simplification arises if we set an equal width of $P/4$ for all the regions in the unit cell. Now we can solve for the Fourier coefficients,

$$a_n = \frac{1}{P}\int_P T(x)\, e^{-2\pi j n\frac{x}{P}}\mathrm{d}x. \tag{8}$$

With the mentioned assumptions, we get the solutions for the zeroth order,

$$a_0 = \frac{1}{2} + \frac{1}{4}e^{j\varphi_1} + \frac{1}{4}e^{j\varphi_3}, \tag{9}$$

and the higher orders,

$$a_n = \frac{1}{\pi n}[(\sin\{\pi n\} - \sin\{0.75\pi n\})e^{j\varphi_1} + [\sin(0.75\pi n) - \sin(0.25\pi n)] + \sin(0.25\pi n)e^{j\varphi_3}]. \tag{10}$$

Now we have analytical equations for the diffraction efficiencies,

$$\eta_n = |a_n|^2, \tag{11}$$

which can be calculated for a range of $\varphi_1 = 0{:}2\pi$ and $\varphi_3 = 0{:}2\pi$. Now we can find the locations of highest uniformity, for example where $|\eta_0 - \eta_1| + |\eta_0 - \eta_2|$ is minimal. If we do so, we find four locations of lowest difference giving a diffraction efficiency of 16.85% in each order. This value is the highest achievable efficiency for the specific number of diffraction orders, defined by the total number of unit cells in each period of the MFL. Table 1 indicates the

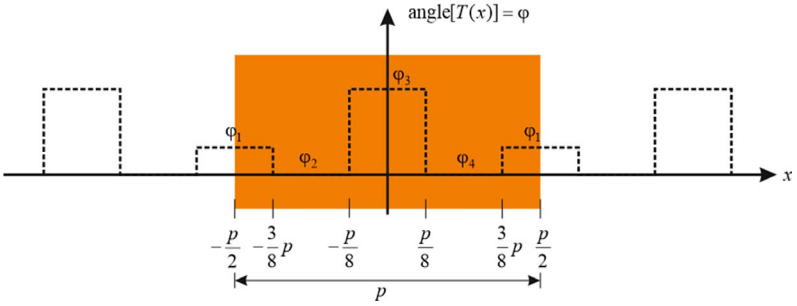

Fig. 2. Configuration of a single grating unit cell with a symmetrical profile with optimized phase values.

Table 1. Possible configurations of phase values assigned to φ_1 and φ_3. Configuration 1 and 2 are exactly the same, the values of 1 and 3 sum up to exactly 2π as well as the values of 2 and 4.

	1	2	3	4
φ_1	1.0694	3.3653	5.2138	2.9179
φ_3	3.3653	1.0694	2.9179	5.2138

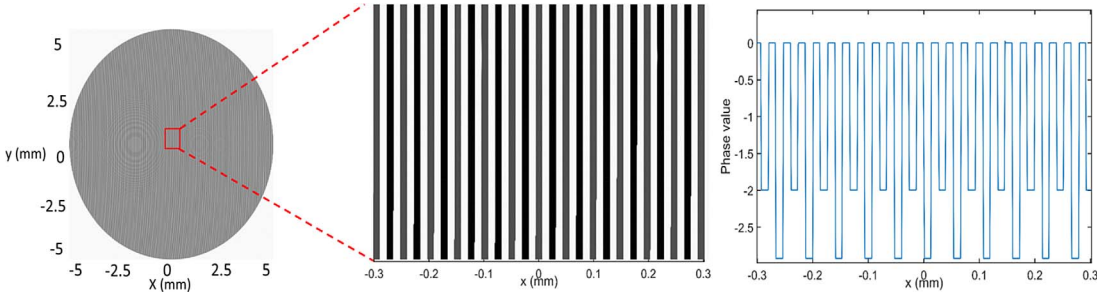

Fig. 3. Pattern of a designed DL with 5 mm radius. (b) Plot of the phase distribution with four phase value (1.07π, 0, 0.34π, 0) in each period of the DOE.

different possible configurations of the phase values assigned to ϕ_1 and ϕ_3. Here, because of an offset, the values are the same in 1 and 2, as well as in 3 and 4.

The pattern shown in Figure 3 demonstrates the DL, designed for 1 mm light sheet distance and 532 nm wavelength of illumination beam by considering a focal length of $f_2 = 13{,}330$ mm in combination with a refractive lens focal length of $f_1 = 100$ mm, period of $p = 0.0532$ mm and a radius of $R = 5$ mm. The incident beam through the DL and a 100 mm focal length refractive lens behind it, is splitted into 5 focal spots in the back focal plane as shown in Figure 4a. The intensity distribution is calculated by a 2D fast Fourier transformation-based Fresnel diffraction integral with a refractive lens, according to,

$$I(\vec{r}, z) = \left| \frac{\exp(jkz)}{j\lambda z} \iint T_{\mathrm{DL}}(\vec{\rho}) \times \exp[j\phi_r(\vec{\rho})] \times \exp\left[\frac{jk}{2z}(\vec{\rho} - \vec{r})^2\right] \mathrm{d}\vec{\rho} \right|^2, \tag{12}$$

where $\vec{r}$ and $\vec{\rho}$ represent the coordinates of observation and DL planes, respectively. z is the propagation distance along the optical axis.

As mentioned above, the platform in the laboratory configuration of LSFM, is filled with water and the incoming laser light is refracted within the tube, between air and water. Therefore, the influence of the water on the positions of the light sheets has also been considered in the design. Since the telecentric arrangement of the system determines that the main incident ray of different orders is parallel to the water, the vertical position of the diffraction orders remains unchanged and is equal to 1 mm. However, the orders are shifted in the horizontal direction. Based on Snell's law,

$$n_a \sin\theta_a = n_w \sin\theta_w, \tag{13}$$

where n_a and θ_a are the refractive index of air and the angle of incidence in the air, n_w and θ_w are the refractive index of water and the angle of incidence in the water, respectively. The relationship between the horizontal relative distances of diffraction orders in the air and the water can be described as (with paraxial approximation),

$$\Delta d_a = \frac{n_a}{n_w} \Delta d_w, \tag{14}$$

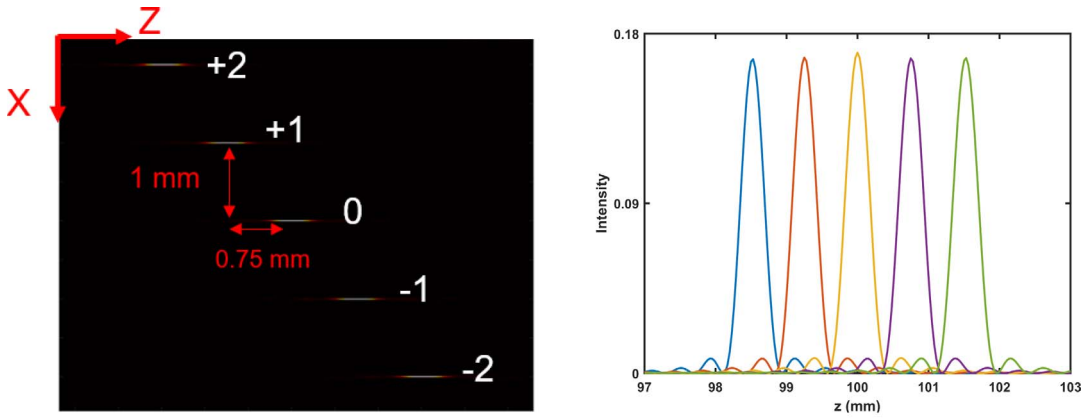

(a) (b)

Fig. 4. Numerical simulation result in Matlab. (a) Side view (XZ plane) of the Five focal spots locating at (98.530, 2), (99.255, 1), (100, 0), (100.756, −1), (101.532, −2). (b) Intensity profile of the focal spots along the optical axis by calculating without $j\lambda z$ in the Fresnel integral.

where Δd_a is the horizontal relative distances of diffraction orders in the air, with $n_a = 1$, $n_w = 1.33$ and the horizontal relative distance of diffraction orders in the water $\Delta d_w = 1$ mm. Thus, the relative horizontal distances of two adjacent diffraction orders in air is designed to be $\Delta d_a \approx 0.75$ mm, as simulated in Figure 4b. The absolute displacement distance of the zero order d_0 as it transitions from the air to the water medium can be determined by,

$$d_0 = L\left(1 - \frac{n_a}{n_w}\right), \tag{15}$$

where the half length of the chamber $L = 11$ mm. Finally, the positions of the higher diffraction orders in water can be determined according to the position of the zero order and the relative distances.

3 Fabrication

The general structure of the designed DL is a slightly curved element with four areas having different phase values, where two of these optimized values are the same as it is mentioned in 1, making it a three step phase element. To fabricate the designed element, one needs to etch down two depths, regarding the phase values of 1.07π and 0.34π. The phase values can be translated into surface-relief etch depths based on,

$$h = \frac{\lambda_0}{2\pi}\frac{\Delta\varphi}{(\Delta n)}, \tag{16}$$

where λ_0 is the wavelength of illumination beam, $\Delta\varphi$ is the phase difference of the two areas, and Δn is the difference in refractive indices of the transmissive DOE material and air. The etch depths in fused silica (SiO_2) for operation with a wavelength of 532 nm are converted from the phase difference values to be 196.3 nm and 617.8 nm, respectively. Two consecutive lithography and reactive ion etching (RIE) steps were carried out. The mask data

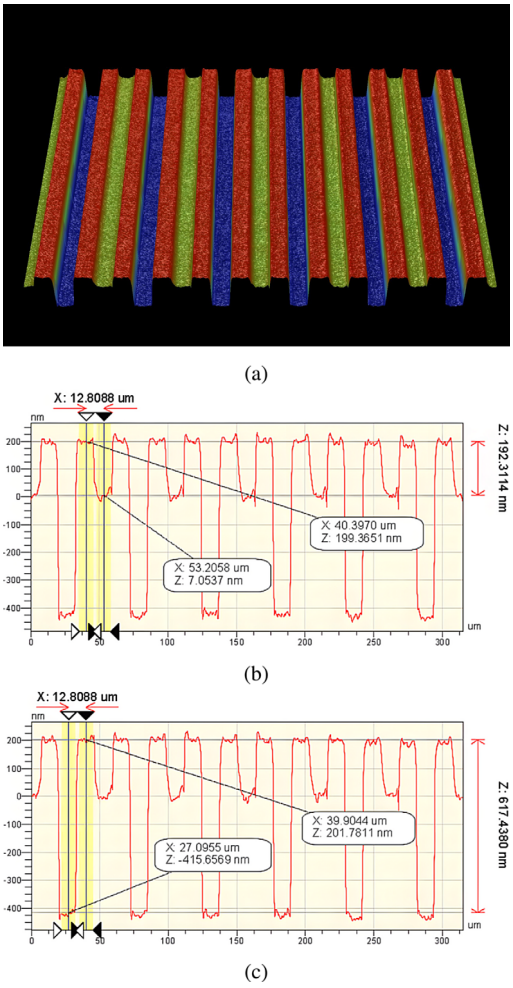

(a) (b) (c)

Fig. 5. (a) 3D impression of the etched structure and false color image (red = 278 nm, blue = −475 nm) taken with white light interferometry (zoom in 20×); (b) and (c) show the scan perpendicular to the grooves giving the etch depths taken with white light interferometry.

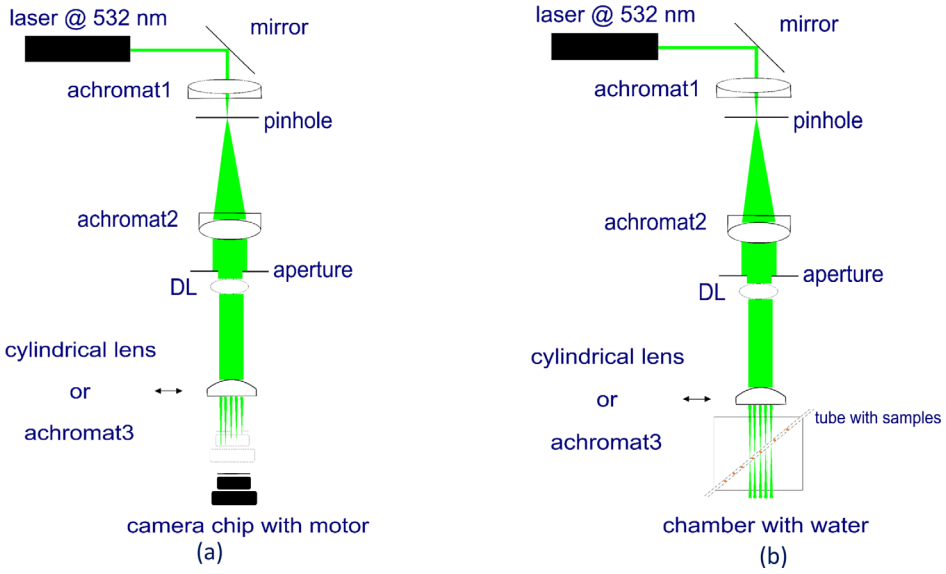

Fig. 6. Schematic of the optical setup to observe: (a) the generated multiple focal spots with a camera chip moving along the optical axis with a motor; (b) the generated multiple light sheets along the tube with samples within the chamber filled with water.

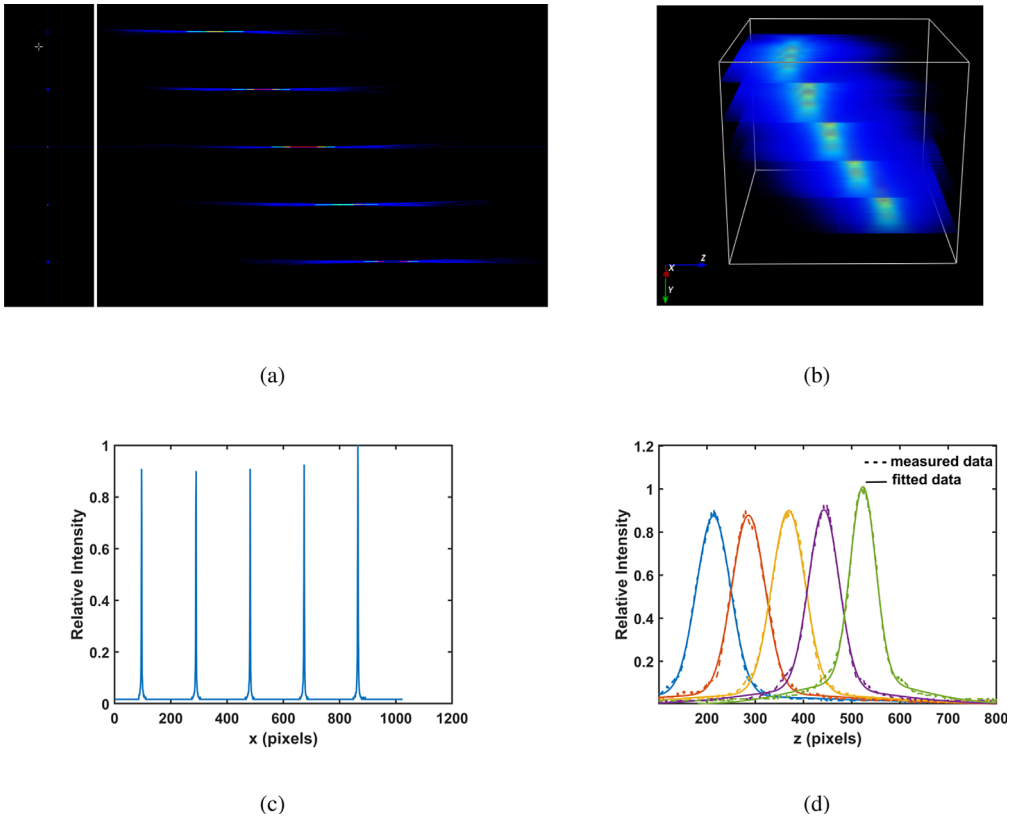

Fig. 7. (a) Display of the five focal spots in the x–z plane. (b) Cube of 6 mm × 6 mm × 6 mm showing the five light-sheets in 3D. (c) 1D Intensity distribution of the normalized intensity distribution in vertical direction (x-axis). (d) The normalized Intensity distribution of measured data, each fitted with a Gaussian function in axial direction (z-axis).

for the lithography using a mask-less aligner (MLA 150, Heidelberg Instruments) was generated with a pixel size of 250 nm × 250 nm. The first lithography and etching step formed the pattern with the smaller etching depth with an etching time of 2 min 27 s. After resist stripping the second lithography and etching step followed with

Table 2. Summary of the calculated and measured focus positions in air and the deviations in x and z.

	Design (air)			Measurement (air)		Deviation	
Order	z/mm	$\lvert\Delta z\rvert$/mm	$\lvert\Delta x\rvert$/mm	$\lvert\Delta z\rvert$/mm	$\lvert\Delta x\rvert$/mm	δx/mm	δz/mm
+2	98.532	1.478	2.000	1.560	2.046	0.03	0.082
+1	99.255	0.745	1.000	0.832	1.018	0.018	0.087
0	100	–	–	–	–	–	–
−1	100.756	0.756	1.000	0.736	1.018	0.018	−0.020
−2	101.532	1.523	2.000	1.536	2.030	0.046	0.013

an etching time of 8 min 14 s. The resulting etching depths were measured with white light interference microscopy to be 194 nm and 628 nm.

The alignment error (maladjustment) of the two etching processes were 100 nm on the x-axis and 50 nm on the y-axis. The smallest feature size was about 12.81 µm according to light microscopy inspection. The results from the examination by white light interference microscopy is shown in Figure 5.

4 Measurement results

The performance of the DL was measured in a first step in air in combination with a symmetrical lens forming focal spots, as illustrated in Figure 6a. A laser beam with a wavelength of 532 nm was expanded by a telescope consisting of a 6 mm, followed by a pinhole for spatial filtering and a 100 mm achromatic lens resulting in a beam diameter of about 14 mm. The focal spot width is experimentally found to be 9 µm at FWHM. The size of the illuminated area on the DOE could be adjusted by an iris stop. It was set to about 7 mm in diameter to ensure that only the patterned area of the DL was illuminated. A refractive lens of 100 mm focal length was placed 100 mm behind the DL to ensure telecentricity of the foci. A bare 8-bit camera chip was mounted onto a motorized linear stage and both elements were controlled via the software Micromanager [24]. The 3D intensity distribution was measured as an image stack along the optical axis (z-stack) for a measuring range of 8 mm. The linear stage moved with a step size of 10 m between consecutive pictures. Figure 7 shows the intensity distribution of the generated axially shifted five focal spots in the x–z-plane by means of the open community platform for bioimage informatics Icy (https://icy.bioimageanalysis.org/) and Figure 7c shows the picture of the tube immerse in water with the five light sheet and two higher orders with lower intensity.

Figures 7d and 7e show the intensity distribution in vertical (x-axis) and horizontal (z-axis) direction, respectively. To this end the maximum values were extracted from the 3D image and plotted into one diagram. The determined locations of maximum intensity are listed in Table 2.

In a next step, as illustrated in Figure 6b, a cylindrical refractive lens was used to produce in combination with the DL, five light sheets, each with a FWHM of 10. Figure 7b shows the intensity distribution in air. To show the functionality of the DL in the real setup the tube inserted into the water filled chamber was filled with a sample consisting of fluorescing spheres (1 diameter) embedded in agarose gel to keep the sample position constant.

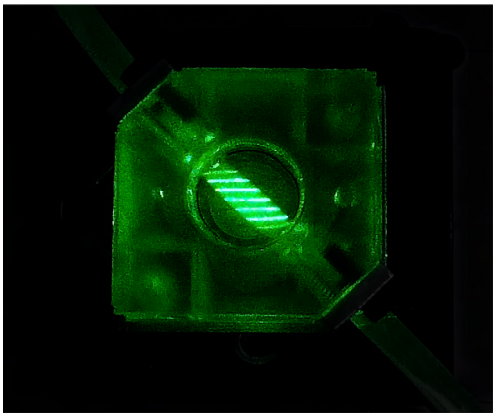

Fig. 8. Measurement chamber with inserted FEP-tube filled with water and illuminated by the multiple light sheets.

Figure 7c shows the top view after carefully aligning the system to ensure that all light sheets are in the center of the tube. By moving the detection system all five light sheets could be made visible by means of the fluorescing particles as a qualitative proof of principle measurement (Fig. 8).

5 Conclusion and outlook

In summary, a diffractive optical element is designed and fabricated for long-term fast 3D imaging of samples using a structured light illumination in LSFM. The design is based on combining a MFL and a LG in a way that the resulting transmission function, DL, is a modulated multifocal diffractive lens and generates multiple light sheets of uniform and equal intensity in combination with a cylindrical lens. One can decide the number of light sheets, their position, distances and their orientation by adjusting the design parameters. In this paper, in a specific configuration the multiple light sheets illuminate an inclined guiding tube of flow driven samples within a specific 3D culture platform. The performance of the DL is demonstrated and measured by illuminating an inclined guiding tube with five light sheets within a three dimensionally adjustable chamber platform of fluorescent sample.

The designed DL can be used not only in the illumination system to form five Light sheets of equal intensity, but also in the imagining system to realize the multi-plane imaging of multiple object planes onto a common camera sensor [10].

Conflict of interest

The authors declare no conflict of interest.

Acknowledgments. We acknowledge support for the publication costs by the Open Access Publication Fund of the Technische Universität Ilmenau.

References

1 Huisken J., Stainier D.Y. (2009) Selective plane illumination microscopy techniques in developmental biology, *Development* **136**, 1963–75.
2 Santi P.A. (2011) Light sheet fluorescence microscopy: A review, *J. Histochem. Cytochem.* **59**, 129–38.
3 Keller P.J., Stelzer E.H. (2010) Digital scanned laser light sheet fluorescence microscopy, *Cold Spring Harb. Protocols* **2010**, pdb–top78.
4 Olarte O.E., Andilla J., Gualda E.J., Loza-Alvarez P. (2018) Light-sheet microscopy: A tutorial, *Adv. Opt. Photon.* **10**, 111–179.
5 Gao L., Shao L., Higgins C.D., Poulton J.S., Peifer M., Davidson M.W., Wu X., Goldstein B., Betzig E. (2012) Noninvasive imaging beyond the diffraction limit of 3D dynamics in thickly fluorescent specimens, *Cell* **151**, 1370–85.
6 Lemke K., Förster T., Römer R., Quade M., Wiedemeier S., Grodrian A., Gastrock G. (2015) A modular segmented-flow platform for 3D cell cultivation, *J. Biotechnol.* **205**, 59–69.
7 Gualda E.J., Pereira H., Vale T., Estrada M.F., Brito C., Moreno N. (2015) Spim-fluid: Open source light-sheet based platform for high-throughput imaging, *Biomed. Opt. Express* **6**, 4447–56.
8 Huang Z., Gu P., Kuang D., Mi P., Feng X. (2021) Dynamic imaging of zebrafish heart with multi-planar light sheet microscopy, *J. Biophoton.* **14**, 5, e202000466. https://doi.org/10.1002/jbio.202000466.
9 ZuninoSanti A. (2021) Multiplane encoded light-sheet microscopy for enhanced 3d imaging, *ACS Photon.* **8**, 3385–3393.
10 Dalgarno P.A., Dalgarno H.I.C., Putoud A., Lambert R., Paterson L., Logan D.C., Towers D.P., Warburton R.J., Greenaway A.H. (2010) Multiplane imaging and three dimensional nanoscale particle tracking in biological microscopy, *Opt. Express* **18**, 877–884.
11 Mohan K., Purnapatra S.B., Mondal P.P. (2014) Three dimensional fluorescence imaging using multiple light-sheet microscopy, *Plos One* **9**, 6, e96551. https://doi.org/10.1371/journal.pone.0096551.
12 Dammann H., Klotz E. (1977) Coherent optical generation and inspection of two-dimensional periodic structures, *Opt. Acta: Int. J. Opt.* **24**, 505–515.
13 O'Shea D.C., Suleski T.J., Kathman A.D., Prather D.W. (2003) *Diffractive optics: Design, fabrication, and test*, SPIE Press Book, Bellingham, Washington USA.
14 Sinzinger S., Jahns J. (2006) *Microoptics*, John Wiley & Sons, Weinheim, Germany.
15 Hofmann M., Ghebjagh S.G., Lemke K., Sinzinger S. (2021) Multi-sheet excitation and imaging of flow driven samples in an LSFM with a modified multi-focal diffractive lens, in: *OSA Imaging and Applied Optics Congress 2021*, Virtual / Digital Format, Optical Society of America, p. CM1A–7.
16 Ghebjagh S.G., Fischer D., Sinzinger S. (2019) Multifocal multi-value phase zone plate for 3D focusing, *Appl. Opt.* **58**, 8943–8949.
17 Soskin M.S., Polyanskii P.V., Arkhelyuk O.O. (2004) Computer-synthesized hologram-based rainbow optical vortices, *New J. Phys.* **6**, 196.
18 Kazanskiy N.L., Khonina S.N., Karpeev S.V., Porfirev A.P. (2020) Diffractive optical elements for multiplexing structured laser beams, *Quant. Electron. (Woodbury, NY)* **50**, 629–635.
19 Khonina S.N., Ustinov A.V., Skidanov R.V., Porfirev A.P. (2015) Local foci of a parabolic binary diffraction lens, *Appl. Opt.* **54**, 5680–5685.
20 Golub M., Doskolovich L., Kazanskiy N., Kharitonov S., Soifer V. (2010) Computer generated diffractive multi-focal lens, *J. Mod. Opt.* **39**, 1245–1251.
21 Suppapitnarm A., Seffen K., Parks G., Clarkson P. (2000) A simulated annealing algorithm for multiobjective optimization, *Eng. Optim.* **33**, 59–85.
22 Brooks S., Morgan B. (1995) Optimization using simulated annealing, *J. Roy. Stat. Soc. Ser. D* **44**, 241–257.
23 Tominaga D., Nobuto K., Masahiro O. (2000) Efficient numerical optimization algorithm based on genetic algorithm for inverse problem, in: *Proceedings of the 2nd Annual Conference on Genetic and Evolutionary Computation, GECCO 2000*, 8–12 July 2000, Las Vegas, pp. 251–258.
24 Edelstein A.D., Tsuchida M.A., Amodaj N., Pinkard H., Vale R.D., Stuurman N. (2014) Advanced methods of microscope control using μManager software, *J. Biol. Methods* **1**, 2, e10. https://doi.org/10.14440/jbm.2014.36.